SENSITIVITY OF CFC-11 UPTAKE TO PHYSICAL INITIAL CONDITIONS AND INTERANNUALLY VARYING SURFACE FORCING IN A GLOBAL OCEAN MODEL

Gokhan Danabasoglu,* Synte Peacock, Keith Lindsay

National Center for Atmospheric Research

P. O. Box 3000, Boulder, CO 80307, USA

and

Daisuke Tsumune

Central Research Institute of Electric Power Industry, Chiba, Japan

05 January 2009

Submitted to *Ocean Modelling*

(Revised)

* *Corresponding author:* Dr. Gokhan Danabasoglu, National Center for Atmospheric Research, P. O. Box 3000, Boulder, CO 80307, USA. e-mail: gokhan@ucar.edu; phone: 1-303-497-1604; fax: 1-303-497-1700.

Abstract

Sensitivity of the oceanic chlorofluorocarbon CFC-11 uptake to physical initial conditions and surface dynamical forcing (heat and salt fluxes and wind stress) is investigated in a global ocean model used in climate studies. Two different initial conditions are used: a solution following a short integration starting with observed temperature and salinity and zero velocities, and the quasi-equilibrium solution of an independent integration. For surface dynamical forcing, recently developed normal-year and interannually varying (1958-2000) data sets are used. The model CFC-11 global and basin inventories, particularly in the normal-year forcing case, are below the observed mean estimates, but they remain within the observational error bars. Column inventory spatial distributions indicate nontrivial differences due to both initial condition and forcing changes, particularly in the northern North Atlantic and Southern Ocean. These differences are larger between forcing sensitivity experiments than between the initial condition cases. The comparisons along the A16N and SR3 WOCE sections also show differences between cases. However, comparisons with observations do not clearly favor a particular case, and model − observation differences remain much larger than model − model differences for all simulations. The choice of initial condition does not significantly change the CFC-11 distributions. Both because of locally large differences between normal-year and interannually varying simulations and because the dynamical and CFC-11 forcing calendars are synchronized, we favor using the more realistic interannually varying forcing in future simulations, given the availability of the forcing data sets.

Keywords: Ocean general circulation model; Modeled CFC-11 uptake; Initial conditions; Surface dynamical forcing.

1. Introduction

The chlorofluorocarbons CFC-11 and CFC-12 have been increasingly utilized in evaluating Ocean General Circulation Models (OGCMs), largely due to i) a good observational data base (the World Ocean Circulation Experiment, WOCE, upon which Global Ocean Data Analysis Project, GLODAP, Key et al. (2004) is largely based), ii) their well-known atmospheric concentrations, and iii) because they are inert in the ocean. These tracers are particularly useful in assessing model mixing processes, ventilation rates, deep water formation, and circulation characteristics. A comparison of thirteen OGCMs with regards to their skills in reproducing observed CFC-11 distributions is presented in Dutay et al. (2002). However, the impact of oceanic physical initial conditions (i.e., initial distributions of temperature, salinity, and velocity) and interannually varying surface dynamical forcing (i.e., heat and salt fluxes and wind stress) on the model CFC-11 distributions remains unclear in the Dutay et al. (2002) study: the models in the inter-comparison study each use their own unique initial conditions and forcing datasets when the CFC-11 forcing starts. To the best of our knowledge, the question of how the initial conditions affect simulated CFC-11 and CFC-12 distributions has not previously been studied.

The sensitivity of the modeled CFC-11 uptake to surface thermohaline forcing is studied in England and Hirst (1997) where surface temperature and salinity are restored to their climatological seasonal cycles using a relatively short time scale. Considering additional sensitivity experiments that employ even shorter time scales or enhanced salinities or both for restoring during winter months in the high-latitude North Atlantic and Southern Ocean, they conclude that the surface thermohaline forcing plays only a minor role in affecting

CFC-11 distributions in contrast with improvements resulting from the inclusion of the Gent and McWilliams (1990) isopycnal transport parameterization instead of a horizontal tracer diffusion formulation. In another study, using a repeat cycle of atmospheric forcing covering 1985-1988 period and enhanced winter-time salinities under sea-ice covered regions in the Southern Ocean, Doney and Hecht (2002) find that the formulation of surface forcing under sea-ice-covered regions can significantly impact oceanic CFC-11 uptake through an influence on model deep-water formation around the Antarctic perimeter. In most studies to date, however, the dynamical forcing used in CFC-11 and CFC-12 simulations has been either restoring to climatological annual- or monthly-mean surface temperature and salinity accompanied by climatological annual- or monthly-mean wind stress or applying repeat cycles of observed atmospheric fields covering a specified period (as in Doney and Hecht 2002) while CFC-11 and CFC-12 surface forcings are constructed to represent the 1938-2000 and 1931-2000 periods, respectively.

In the present study, our goal is to explore and quantify the sensitivity of the oceanic CFC-11 uptake to initial conditions and choice of surface dynamical forcing in an OGCM. We note that our simulations also carry CFC-12 and that we choose to show only CFC-11 distributions here, because the results are nearly identical when CFC-12 is used instead. The initial condition issue is becoming more important as the OGCMs used in climate studies increase their resolution – but still largely remain non-eddy-resolving – and obtaining an equilibrium solution becomes prohibitively expensive. Two popular model initialization choices in the literature are observed temperature and salinity with zero velocities, or a quasi-equilibrium state from another simulation, and it is sensitivity of the solution to these initial conditions that we explore here. For the surface dynamical forcing sensitivity, we

consider the recently developed data sets from Large and Yeager (2004, hereafter LY) and use both the interannually varying and normal-year forcing data. These forcing data sets have been recently proposed as common atmospheric forcing data for Coordinated Ocean-ice Reference Experiments (COREs) to investigate the behaviors of global ocean and ocean−sea-ice simulations (Griffies et al. 2008). The present effort is intended to help guide subsequent ocean-model studies that may also choose to use the LY forcing data. We note that the same interannual data set was used in Gent et al. (2006) in their ocean-only CFC-11 simulation. We present brief descriptions of the ocean model and surface forcing as well as a discussion of initial condition differences in section 2. The results are given in section 3. Section 4 includes a summary and discussion.

2. Ocean model, surface forcing, and initial conditions

The model is the ocean component of the National Center for Atmospheric Research (NCAR) Community Climate System Model version 3 (CCSM3) and is based on the Parallel Ocean Program of the Los Alamos National Laboratory (Smith and Gent 2004). In this study, we use the nominal 1° horizontal resolution version of the model. The present model includes the near-surface eddy flux parameterization as implemented by Danabasoglu et al. (2008). Further details of the model set-up and parameterizations, including the eddy diffusivity and viscosity values are given in Danabasoglu et al. (2006) and references therein.

The surface fluxes of heat, salt, and momentum are evaluated using the bulk forcing method described in Large et al. (1997) and LY. We use both the interannually varying (IAF) and the normal year (NYF) data sets developed by LY. IAF represents a 43-year forcing cycle covering the 1958-2000 period. NYF consists of single annual cycles of all the needed fields constructed from the IAF data to produce similar mean fluxes as the

IAF set. The surface CFC-11 and CFC-12 fluxes are calculated for the 1931-2000 period, following the Ocean Carbon Model Intercomparison Project (OCMIP-2) protocols (Dutay et al. 2002). However, instead of the protocol specified fields, we use the LY atmospheric data sets in these flux equations.

In the present study, we do not use an active sea-ice model. Instead, we prescribe sea-ice fraction using a daily observed data set from Comiso (1999). This data set uses a bootstrap algorithm data product based on the Nimbus-7 Scanning Multichannel Microwave Radiometer prior to 1988, and the Special Sensor Microwave / Imager from 1988 to 2000. In NYF, the daily sea-ice extent is obtained as an average of the 1978-2000 data. In these sea-ice covered regions, wind stress passes directly through the sea-ice. The ocean model is allowed to form frazil ice to keep its surface temperature from falling below freezing in regions where there is no observed ice. In such situations, the surface water is heated to the freezing point with a corresponding increase in salt, representing brine rejection due to ice formation. This kind of ice is not transported, and is melted locally before the surface temperature can rise above freezing temperature again. The heat fluxes due to basal ice formation and penetrating short-wave are set to zero, but the freshwater fluxes associated with the former are prescribed as monthly-mean freshwater fluxes diagnosed from an ocean−sea-ice coupled integration. A weak salinity restoring to the Polar Science Center Hydrographic Climatology (PHC2) data (a blending of Levitus et al. (1998) and Steele et al. (2001) data sets) with a 4-year time scale over 50 m is applied globally with its global-mean subtracted. The salinity enhancements along the Antarctic coast described in Doney and Hecht (2002) are included in the restoring data set. A global precipitation correction factor is computed for each year based on the change of the global-mean salinity during that year.

This factor is used to multiply the precipitation and runoff fluxes during the next year to partially balance evaporation.

Our first experiment (IAF1) is forced with the IAF data and is initialized using the January-mean temperature and salinity from the PHC2 climatology and zero velocity. IAF1 is integrated for 3 repeat cycles of the IAF data to model year 129, i.e., the end of calendar year 2000. The CFC-12 and CFC-11 surface fluxes are introduced in model years 60 and 67, respectively. These model years correspond to calendar years 1974 and 1981, respectively, for the surface fluxes of heat, salt, and momentum in the IAF data cycle, while they correspond to calendar year 1931 for CFC-12 and calendar year 1938 for CFC-11 surface fluxes. Therefore, the calendar years for the atmospheric data used in all surface flux calculations are identical, i.e., synchronous, only during the third cycle of the IAF data, corresponding to calendar years 1958-2000. In other words, only during this integration segment the surface fluxes of heat, salt, momentum, CFC-11, and CFC-12 follow the same calendar years. The second experiment (IAF2) is forced identically with the IAF data, but is initialized from the end state of a 441-year independent simulation with NYF. We note that surface and intermediate waters are in quasi-equilibrium after 441 years, but most deep waters certainly are not. IAF2 is a 70-year integration to the end of calendar year 2000 in which the CFC-11 and CFC-12 are introduced right from the beginning in years 1 and 8, respectively. Here, the first model year corresponds to 1974 in the IAF data cycle for the heat, salt, and momentum fluxes and to 1931 for the CFC-12 surface fluxes. Thus, as in IAF1, all surface fluxes in IAF2 follow the same calendar years for the atmospheric data only during the last 43 years of integration, corresponding to calendar years 1958-2000. Finally, experiment NYF2 is identical to IAF2, except that it is forced with the NYF data. In each experiment,

the initial CFC-11 and CFC-12 concentrations are set to zero.

The initial conditions considered here represent reasonable and practical choices, typical of those adopted in ocean modeling community. To show a measure of the initial condition differences before the CFC-11 surface fluxes are introduced, we present the annual- and zonal-mean potential density difference distributions obtained by subtracting model year 60 of IAF1 from model year 1 of IAF2 in Figs. 1a and b for the Atlantic + Arctic and Pacific + Southern Ocean basins, respectively. This figure reveals that IAF2 generally has lighter waters in the upper ocean and denser waters in the deeper ocean, relative to IAF1. The largest differences are in excess of 0.5 kg m^{-3}, occurring in the near-surface Arctic Ocean. In the North Atlantic, the differences reach 0.3 kg m^{-3} near the surface. The Antarctic Intermediate Water densities in IAF2 are lighter by as much as 0.15 kg m^{-3} than in IAF1. There is some large scale density compensation occurring in the corresponding annual- and zonal-mean temperature and salinity distributions (not shown), e.g., between the equator and 30°S in the 150 to 2000-m depth range in the South Atlantic, IAF2 is warmer and saltier by as much as 1.8°C and 0.35 psu, respectively, than in IAF1. By construction of our salinity forcing, the global-mean salinity in both cases are nearly identical. In IAF2, the Atlantic basin is generally warmer and the Indian-Pacific basin is generally cooler than in IAF1. As a result of these compensations, the global-mean temperatures are similar in IAF1 (3.64°C) and IAF2 (3.62°C). There are also differences in ocean circulation between the two initial conditions for IAF1 and IAF2. The Antarctic Circumpolar Current (ACC) transports at the Drake Passage are 150 and 128 Sv in IAF1 and IAF2, respectively. The subpolar gyre in the North Atlantic is stronger by as much as 5 Sv in IAF2 than in IAF1. The maximum transports of the meridional overturning cell associated with the North Atlantic

Deep Water (NADW) are 19 and 17.3 Sv in IAF1 and IAF2, respectively. Similarly, the meridional overturning cell associated with the Antarctic Bottom Water (AABW) has a larger maximum transport in IAF1 (16.4 Sv) than in IAF2 (13.3 Sv). Further discussions on initial conditions and final states of these two cases are given in section 4.

3. Results

Figure 2 shows the time evolution of the CFC-11 inventory starting at 1950 for the three cases. The figure includes observational estimates with error bars from Willey et al. (2004) and GLODAP (Key et al. 2004) centered around 1994. Because the GLODAP dataset excludes some adjacent seas (e.g., the Mediterranean Sea) and the Arctic Ocean, inventory time series without the Arctic Ocean and the model marginal seas (i.e., the Mediterranean, Red, Baltic, Black, and Caspian Seas, Persian Gulf, and Hudson Bay) are also presented in Fig. 2. CFC-11 uptake in the interannual forcing cases is nearly identical. In comparison with these cases, NYF2 shows somewhat lower uptake particularly noticeable after 1987. In 1994, all the model inventories are below the observational mean estimates, but they remain within their error bars. We note that the exclusion of the Arctic Ocean alone reduces the model inventories by 0.3×10^8 moles, corresponding to 6% of the global-mean inventory of 4.99×10^8 moles for 1994 in IAF1 and IAF2 (see Table 1). This contribution of the Arctic Ocean is consistent with the observational estimates of Willey et al. (2004) and Tanhua et al. (2009) where the Arctic Ocean inventory estimates are 0.28×10^8 and 0.26×10^8 moles, respectively, representing about 5% of the global-mean inventory of 5.5×10^8 moles for 1994. The contribution from the model marginal seas to the global inventory is negligible, i.e., about 0.8% of the global inventory.

We provide the basin and global CFC-11 inventories for 1994 from the model simu-

lations and observational estimates in Table 1. To facilitate comparison with the Willey et al. (2004) observational estimates, the Indian, Pacific, and Atlantic basins include their respective Southern Ocean sectors. With the exception of the Arctic Ocean, all model solutions underestimate the CFC-11 uptake in all basins. The worst magnitude (0.26-0.31$\times 10^8$ moles) and percentage (19-21%) deficits in comparison with the observations occur in the Atlantic and Indian basins, respectively. Consequently, the Pacific basin shows the best agreement with the observations. In comparison with the interannually forced cases, the NYF2 CFC-11 inventory is consistently lower in the Atlantic, Pacific, and Indian basins, thus resulting in 0.12×10^8 moles lower global inventory. Nevertheless, the NYF2 global inventory still remains within the observational error bars.

As another integrated measure of the oceanic CFC-11 uptake, Fig. 3 shows the zonal-mean CFC-11 column inventories from the model simulations in comparison with the GLODAP data for year 1994. In addition to the global zonal-mean, the Atlantic, Pacific, and Indian Ocean zonal-means are also included in the figure. With the exception of a few latitude bands, e.g., north of 45°N in the Pacific Ocean and extreme northern Indian Ocean, the model CFC-11 uptake is slightly below the observational estimates at all latitudes. The IAF1 and IAF2 zonal-means are mostly indistinguishable from each other. The lower CFC-11 inventory in NYF2 compared to in IAF1 and IAF2 is particularly noticeable in the Southern Ocean latitudes as well as between 25°-60°N in the Pacific Ocean.

To expose spatial distribution details, the CFC-11 column inventory distributions for year 1994 are presented from the GLODAP data and IAF2 in Fig. 4. Both here and in Fig. 5, IAF2 is chosen as a reference case and the changes due to initial condition and forcing are shown as IAF2 − IAF1 and IAF2 − NYF2 difference distributions, respectively.

The model cases reproduce the general features of the GLODAP data. However, as in Gent et al. (2006), the modeled column inventories remain somewhat lower than observed in the tropical Pacific and Atlantic, in the North Pacific, and along the ACC path, and higher than observed in the Northwestern Atlantic. Sensitivities to initial condition and forcing, in terms of their effects on the CFC-11 inventory, are largest in the Arctic Ocean. Unfortunately, whether these changes in spatial distributions represent improvements or not remain unclear due to extremely limited observational data there. Elsewhere, the impacts of initial conditions are relatively small and somewhat mixed in comparison with observations. For example, smaller values in the Labrador Sea and higher values off the North American coast at about 30°N produce better comparisons with observations in IAF2 than in IAF1. However, smaller values south of Newfoundland and larger values in the Eastern Atlantic north of 45°N degrade the comparison with observations in IAF2.

In contrast to initial condition comparisons, there are larger differences between the forcing experiments (NYF2 vs. IAF2). With the IAF data, the column inventory increases in the North Pacific and particularly along the ACC path (by about 10%) over the NYF, thus noticeably improving comparisons with observations. Generally smaller magnitudes of the CFC-11 column inventory off the Antarctic coast, including the Weddell Sea region, however, are found with the IAF, creating further departures from observations in IAF2 than in NYF2. Increased column inventory in the North Atlantic north of 30°N with IAF improves the model simulation south of 45°N while slightly degrading the comparison with observations further north. These changes reflect the variability associated with the interannual forcing. For example, higher CFC-11 uptake along the ACC path is likely due to generally larger values of the zonal wind stress in the 1990s – represented in the IAF – compared to the NYF

data set. In 1994, somewhat lower surface temperatures also contribute to this increased uptake here. Ultimately what matters for an increased CFC-11 uptake is a correlation between high surface wind stress, low surface temperatures, and high atmospheric CFC-11 concentrations. Another commonly used measure of CFC-11 uptake is the penetration depth defined as the column inventory divided by the surface concentration (Dutay et al. 2002). The comparisons of the penetration depth distributions show similar differences as in column inventories between model experiments and observations (not shown).

Figure 5 shows the observed and modeled CFC-11 distributions along the WOCE A16N (20°W) and SR3 (140°E) sections. These observations were taken in August 1993 and October 1991, respectively, and we use the same months and years from the model simulations in the following comparisons. The figure also includes IAF2 − WOCE, IAF2 − IAF1, and IAF2 − NYF2 difference distributions for both sections. For these comparisons, both the WOCE and model CFC-11 data are interpolated to a common grid that differs from both the observational and model grids. The model − model CFC-11 concentration differences along these sections (Figs. 5g-j) represent typical values in the northern North Atlantic and Southern Ocean, where the largest differences among model experiments are seen (Fig. 4). By comparison, in the low- and mid-latitude oceans, the CFC-11 distribution differences between cases are considerably smaller ($< 10\%$), and the model and WOCE section distributions are in good agreement. While all three simulations show the same general features as observed along the A16N and SR3 sections, there are several prominent and rather large magnitude differences from observations. For example, simulated CFC-11 remains too low by more than 1 pmol kg^{-1} between 500 and 1000-m depth north of 40°N along the A16N section in all model experiments (e.g., Fig. 5e). In contrast, the model CFC-11 concentra-

tions are too high by as much as 1.6 pmol kg^{-1} below 1000-m depth north of 40°N along the same section. Gent et al. (2006) attribute these model errors to the incorrect path of the modeled North Atlantic Current and anomalous advection of high CFC-11 waters from the western North Atlantic. These model shortcomings also exist in the present simulations. Other examples of significant model CFC-11 deficiencies include the higher than observed (by more than 1 pmol kg^{-1}) upper-ocean concentrations as well as the low bias in excess of 1 pmol kg^{-1} along the southern topography along the SR3 section (Fig. 5f). The latter bias indicates that the model does not form enough deep water here. Doney and Hecht (2002) show strong sensitivity of the deep water formation off Antarctica to the salinity values used in their under sea-ice restoring term. Although we use their salinity enhancements in the restoring data set in the present study, our restoring time scale is much longer than the one used in their work. This weaker salinity restoring is the likely culprit for reduced deep water formation along the SR3 section than observed, implied by the lower model CFC-11 concentrations at depth. The reason for the high upper-ocean CFC-11 concentrations largely remains unclear as the model temperature distributions show differences of up to 1°C (both signs) from observations. However, we speculate that the reduced deep water formation and a mixed layer deep bias along the SR3 section lead to excess northward transport of CFC-11 along isopcynals, thus contributing to the larger model CFC-11 uptake in the upper-ocean.

Figures 5g-j reveal that the model − model differences remain much smaller than the model − observation differences. To provide a quantitative comparison, Table 2 shows the root-mean-square (rms) of the model − WOCE and model − model differences for all cases along the A16N and SR3 sections. While the individual model rms differences from observations are in the range of 0.38-0.44 pmol kg^{-1}, the IAF2−IAF1 and IAF2−NYF2

rms differences remain much smaller at 0.10-0.14 pmol kg^{-1}, representing about 25-37% of the model − observation rms differences. Although the IAF2−WOCE rms differences are slightly higher than the ones for IAF1−WOCE and NYF2−WOCE, these section comparisons do not clearly favor a particular case.

4. Summary and discussion

We have investigated the sensitivity of the oceanic CFC uptake to initial conditions and interannually varying surface dynamical forcing in the ocean component of the NCAR CCSM, focusing on the CFC-11 distributions. We have considered two initial condition sets prior to the introduction of CFC-11 surface fluxes: a quasi-equilibrium solution obtained separately and a state following a short integration starting from observed buoyancy field and state of rest. These represent reasonable and practical choices for ocean initialization. We have used both the interannually varying (1958-2000) and normal year data sets developed by LY, recently proposed as common atmospheric forcing data for CORE (Griffies et al. 2008). The model CFC-11 global and basin inventories, particularly with the normal-year forcing, are below the observed mean estimates, but they remain within the observational error bars. Column inventory spatial distribution comparisons indicate nontrivial differences due to both initial condition and forcing changes, particularly in the northern North Atlantic and Southern Ocean. These differences are larger between forcing sensitivity experiments than between the initial condition experiments. The comparisons along the A16N and SR3 WOCE sections also reveal nontrivial differences between experiments, but do not clearly favor a particular case. Nevertheless, because of these locally large differences between cases, we recommend that future model inter-comparison studies should specify a common atmospheric dataset – to be used by all participating models – as a part of their protocols

to at least eliminate differences in forcing.

Unfortunately, model − observation differences remain larger than model − model differences. Therefore, we conclude that the different initial conditions and surface forcing data considered here have only secondary effects on the CFC-11 distributions. The changes in model physics and parameters as well as different treatments of under sea-ice forcing (Doney and Hecht 2002) are expected to have more significant impacts on model CFC-11 distributions and model − observation comparisons. A similar conclusion was stated in England and Hirst (1997). Our newer model which has improved physical parameterizations still suffers from unsatisfactory CFC-11 simulations. We believe that persistent model deficiencies associated with deep water formation (i.e., AABW), Antarctic Intermediate Water, and Sub-Antarctic Mode Water play significant roles in the model underestimates of the mean CFC-11 uptake. Significantly different surface forcing than used here can lead to better comparisons with observations. For example, restoring of surface salinity to modified data sets with short time scales as in England and Hirst (1997) and Doney and Hecht (2002) or stronger zonal wind stress of a coupled simulation than in observations as in Gent et al. (2006) can produce better CFC-11 distributions, particularly in the Southern Ocean. However, while the latter represents a coupled model bias, the former is a traditional, but unphysical approach, and resulting CFC-11 improvements are likely for the wrong reasons. We believe that our under sea-ice forcing methodology described in section 2 is somewhat better than applying particularly strong temperature and salinity restoring in these regions, but still remains rather ad-hoc. Griffies et al. (2008) advocate always using coupled ocean − sea-ice models in evaluation of the ocean models. While this approach largely eliminates the under sea-ice forcing problems, it creates some others. These include added complexity

of a prognostic sea-ice model and its fidelity and, perhaps most importantly, the lack of feedbacks onto a prescribed atmosphere when the model and forcing errors produce simulated sea-ice cover that deviates significantly from the one used to create the atmospheric state (see sections 2 and 3 of Griffies et al. 2008 for further details). In addition, it is important to note that using a sea-ice model does not automatically improve an ocean model's deep water formation (Dutay et al. 2002). Because model CFC-11 local distributions are clearly sensitive to interannual variability in forcing, and because the dynamical and CFC-11 forcing calendars are synchronized in the more realistic interannual forcing, we favor using this forcing in future simulations, given the availability of the data sets.

The relatively small sensitivity of the model CFC-11 uptake to the oceanic initial conditions is largely due to the rapid adjustment (on decadal time scales) of the upper-ocean density field to the surface buoyancy forcing as shown in Figs. 1c and d. These panels present the decadal-mean potential density differences between IAF1 and IAF2 for the last decade of integrations, showing that the differences are significantly smaller then the initial condition differences given in Figs. 1a and b. During the time over which the density differences between the cases are larger, the atmospheric CFC-11 concentrations are too small to impact the oceanic CFC-11 inventory. In contrast, as the atmospheric concentrations increase towards the end of the Twentieth Century, the density differences diminish between the two cases, thus contributing to the rather similar CFC-11 distributions during the observational comparison period. In addition, most barotropic and meridional overturning transport differences between IAF1 and IAF2 also diminish by the end of the integrations. For example, the NADW circulation differs between IAF1 and IAF2 by only 0.5-1.0 Sv between 1000 and 3000-m depth during the last decade. We do not expect to find considerable

CFC-11 sensitivity to such order 1 Sv NADW local transport differences. This is because the various components of the NADW (combined) are responsible for only about 10% of the total global oceanic CFC-11 uptake as demonstrated in a recent observational study by LeBel et al. (2008). In contrast, the AABW transport remains higher in IAF1 than in IAF2 by as much as 2.5 Sv during the last decade. The impact of this transport difference on the model CFC-11 uptake is small because the CFC-11 concentrations are rather low below about 3000-m depth.

Acknowledgments Two anonymous reviewers provided very relevant comments and suggestions, which greatly improved the final version of the paper. NCAR is sponsored by the National Science Foundation.

References

Comiso, J., 1999 (updated 2002): Bootstrap sea ice concentrations for NIMBUS-7 SMMR and DMSP SSM/I. National Snow and Ice Data Center, Boulder, CO, USA. Digital media. Available from http://nsidc.org/data/nsidc-0079.html.

Danabasoglu, G., R. Ferrari, and J. C. McWilliams, 2008: Sensitivity of an ocean general circulation model to a parameterization of near-surface eddy fluxes. *J. Climate*, **21**, 1192-1208.

Danabasoglu, G., W. G. Large, J. J. Tribbia, P. R. Gent, B. P. Briegleb, and J. C. McWilliams, 2006: Diurnal coupling in the tropical oceans of CCSM3. *J. Climate*, **19**, 2347-2365.

Doney, S. C., and M. W. Hecht, 2002: Antarctic bottom water formation and deep-water chlorofluorocarbon distributions in a global ocean climate model. *J. Phys. Oceanogr.*, **32**, 1642-1666.

Dutay, J.-C., and Coauthors, 2002: Evaluation of ocean model ventilation with CFC-11: Comparison of 13 global ocean models. *Ocean Modelling*, **4**, 89-120.

England, M. H., and A. C. Hirst, 1997: Chlorofluorocarbon uptake in a world ocean model 2. Sensitivity to surface thermohaline forcing and subsurface mixing parameterizations. *J. Geophys. Res.*, **102**, 15709-15731.

Gent, P. R., and J. C. McWilliams, 1990: Isopycnal mixing in ocean circulation models. *J. Phys. Oceanogr.*, **20**, 150-155.

Gent, P. R., F. O. Bryan, G. Danabasoglu, K. Lindsay, D. Tsumune, M. W. Hecht, and

S. C. Doney, 2006: Ocean chlorofluorocarbon and heat uptake during the Twentieth Century in the CCSM3. *J. Climate*, **19**, 2366-2381.

Griffies, S. M., and Coauthors, 2008: Coordinated Ocean-ice Reference Experiments (COREs). *Ocean Modelling* (in press).

Key, R. M., and Coauthors, 2004: A global ocean carbon climatology: Results from Global Data Analysis Project (GLODAP). *Global Biogeochemical Cycles*, **18**, GB4031, doi: 10.1029/2004GB002247.

Large, W. G., and S. G. Yeager, 2004: Diurnal to decadal global forcing for ocean and sea-ice models. The data sets and flux climatologies. *NCAR Tech. Note*, NCAR/TN-460 + STR, 105 pp. (Available online at http://www.cgd.ucar.edu/oce/pubs/04pubs.html).

Large, W. G, G. Danabasoglu, S. C. Doney, J. C. McWilliams, 1997: Sensitivity to surface forcing and boundary layer mixing in a global ocean model: Annual-mean climatology. *J. Phys. Oceanogr.*, **27**, 2418-2447.

LeBel, D. A., and Coauthors, 2008: The formation rate of North Atlantic Deep Water and Eighteen Degree Water calculated from CFC-11 inventories observed during WOCE. *Deep-Sea Res. I*, **55**, 891-910.

Levitus, S., and Coauthors, 1998: Introduction. Vol. 1, World Ocean Database 1998, NOAA Atlas NESDIS 18, 346 pp.

Smith, R. D., and P. R. Gent, 2004: Reference manual for the Parallel Ocean Program (POP): Ocean component of the Community Climate System Model (CCSM2.0 and 3.0). *Tech. Rep. LA-UR-02-2484*, Los Alamos National Laboratory, Los Alamos, NM, 75 pp. (Available online at http://www.ccsm.ucar.edu/models/ccsm3.0/pop).

Steele, M., R. Morley, W. Ermold, 2001: PHC: A global ocean hydrography with a high quality Arctic Ocean. *J. Climate*, **14**, 2079-2087.

Tanhua, T., E. P. Jones, E. Jeansson, S. Jutterström, W. M. Smethie Jr., D. W. R. Wallace, and L. G. Anderson, 2009: Ventilation of the Arctic Ocean: Mean ages and inventories of anthropogenic CO_2 and CFC-11. *J. Geophys. Res.*, **114**, C01002, doi:10.1029/2008JC004868.

Willey, D. A., R. A. Fine, R. E. Sonnerup, J. L. Bullister, W. M. Smethie Jr., and M. J. Warner, 2004: Global oceanic chlorofluorocarbon inventory. *Geophys. Res. Lett.*, **31**, L01303, doi:10.1029/2003/GL018816.

Figure Captions

1. Time- and zonal-mean potential density (referenced to surface) IAF2 minus IAF1 difference distributions. Initial condition differences for a) Atlantic and Arctic and b) Pacific and Southern Oceans and last decade differences for c) Atlantic and Arctic and d) Pacific and Southern Oceans. The basin boundaries are indicated by vertical lines. The contour intervals are 5×10^{-2} and 20×10^{-2} kg m^{-3} for differences of less and greater than 30×10^{-2} kg m^{-3}, respectively. The thin lines and shading indicate negative differences.

2. Time series of the CFC-11 global inventory (thick lines). The thin lines show the inventory excluding the Arctic Ocean and marginal seas. Willey et al. (2004) and Key et al. (2004) observational estimates centered around 1994 are also shown with their respective error bars. The upper Willey et al. (2004) estimate of 5.5×10^8 moles is for the global ocean. The lower Willey et al. (2004) and Key et al. (2004) estimates do not include some adjacent seas and the Arctic Ocean, and their time axis are slightly shifted to prevent overlap. Note that IAF1 and IAF2 lines overlap.

3. Zonal-mean CFC-11 column inventory for 1994 from model simulations and GLODAP data: a) Global, b) Atlantic, c) Pacific, and d) Indian Oceans.

4. CFC-11 column inventory in moles km^{-2} for 1994 from a) GLODAP and b) IAF2; the model difference distributions for c) IAF2 − IAF1 and d) IAF2 − NYF2. Panels (a,b) and (c,d) share the same color bars, respectively.

5. Observed and modeled CFC-11 distributions along WOCE sections A16N (20°W) for August 1993 (left panels) and SR3 (140°E) for October 1991 (right panels). For each

section, IAF2 distribution along with IAF2 − WOCE, IAF2 − IAF1 and IAF2 − NYF2 difference distributions are shown. The unit is pmol kg^{-1}. Panels (a-d) and (e-j) share the same color bars, respectively. All panels use the same, observed topography.

Table 1. Basin and global CFC-11 inventories in 10^8 moles for 1994 from the model simulations and observational estimates. To facilitate comparison with the Willey et al. (2004) observational estimates, the Indian, Pacific, and Atlantic basins include their respective Southern Ocean sectors. The global inventories given in parentheses include the model marginal seas. Key et al. (2004) global estimate does not include the Arctic Ocean. Also, we note that the sum of the computed basin inventories using the GLODAP data (5.33×10^8 moles) is slightly below the global inventory mean (5.4×10^8 moles) given in Key et al. (2004).

Case	Indian	Pacific	Atlantic	Arctic	Global
IAF1	0.90	2.11	1.64	0.30	4.95 (4.99)
IAF2	0.90	2.12	1.64	0.30	4.95 (4.99)
NYF2	0.88	2.04	1.59	0.32	4.83 (4.87)
Willey et al (2004)	1.1	2.2	1.9	0.28	5.5±1.2
GLODAP (Key et al. 2004)	1.13	2.29	1.91		5.4±0.8
Tanhua et al. (2009)				0.26±0.03	

Table 2. The root-mean-square (rms) of the model − WOCE and model − model differences for all cases along the A16N and SR3 WOCE sections. The observations were taken in August 1993 and October 1991 for the A16N and SR3 sections, respectively, and we use the same months and years from the model simulations. The unit is pmol kg^{-1}.

rms difference	A16N	SR3
IAF1−WOCE	0.40	0.40
IAF2−WOCE	0.42	0.44
NYF2−WOCE	0.38	0.41
IAF2−IAF1	0.11	0.10
IAF2−NYF2	0.14	0.12

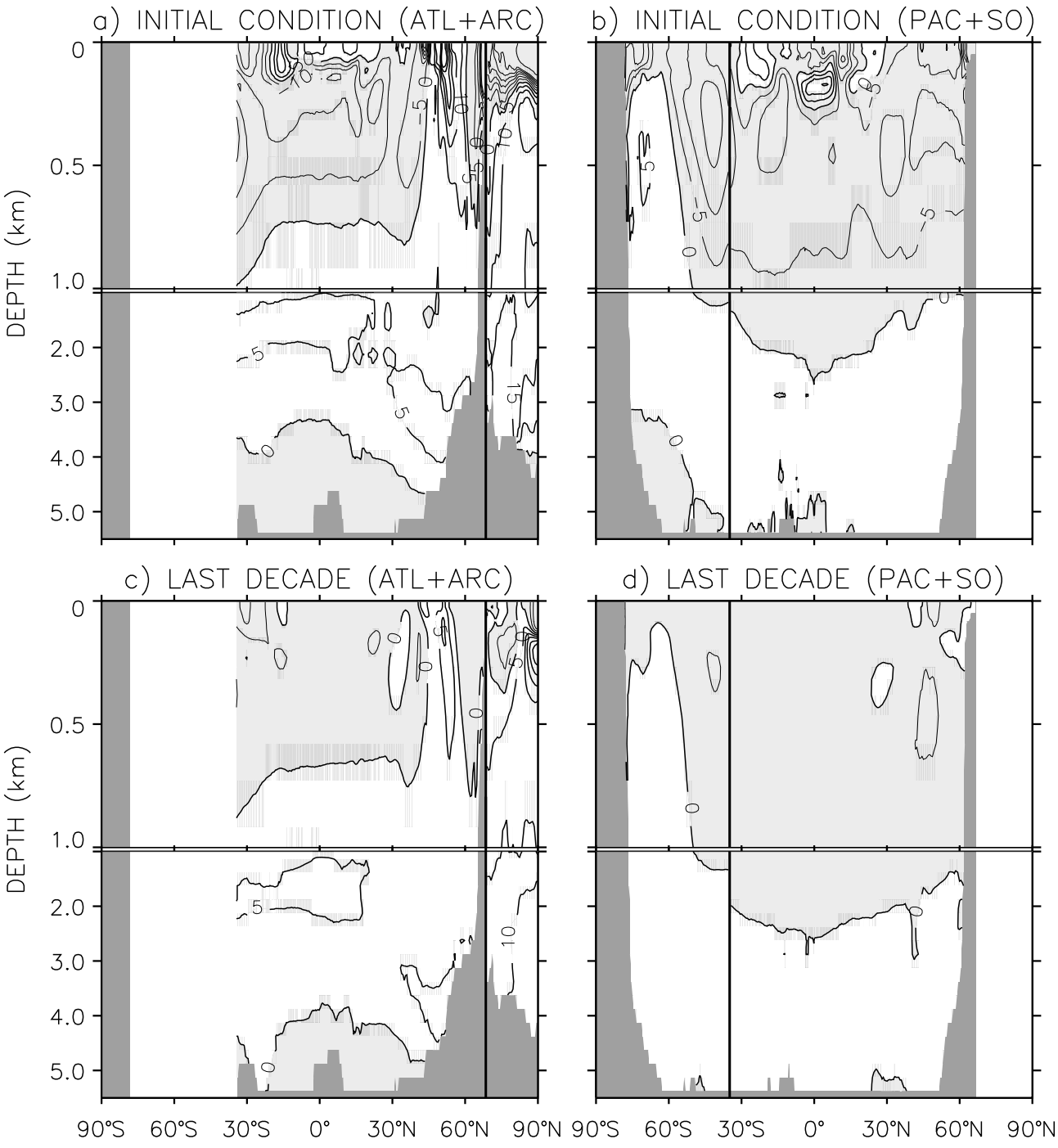

Figure 1. Time- and zonal-mean potential density (referenced to surface) IAF2 minus IAF1 difference distributions. Initial condition differences for a) Atlantic and Arctic and b) Pacific and Southern Oceans and last decade differences for c) Atlantic and Arctic and d) Pacific and Southern Oceans. The basin boundaries are indicated by vertical lines. The contour intervals are 5×10^{-2} and 20×10^{-2} kg m^{-3} for differences of less and greater than 30×10^{-2} kg m^{-3}, respectively. The thin lines and shading indicate negative differences.

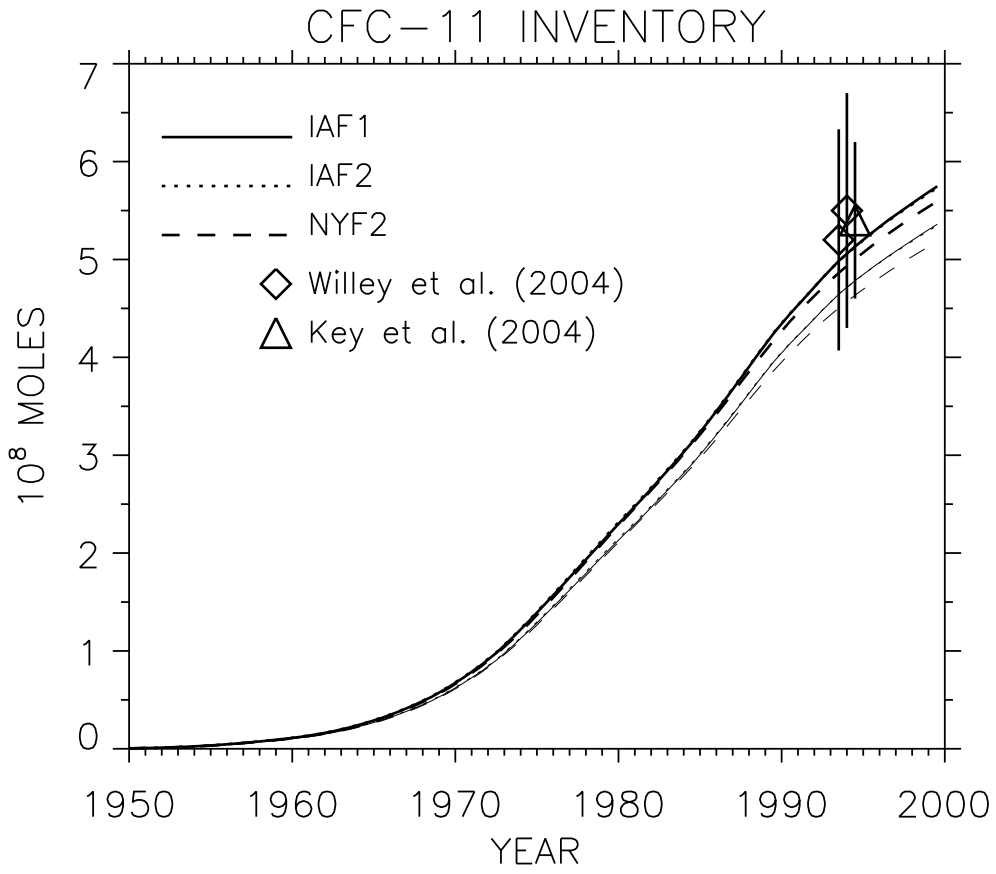

Figure 2. Time series of the CFC-11 global inventory (thick lines). The thin lines show the inventory excluding the Arctic Ocean and marginal seas. Willey et al. (2004) and Key et al. (2004) observational estimates centered around 1994 are also shown with their respective error bars. The upper Willey et al. (2004) estimate of 5.5×10^8 moles is for the global ocean. The lower Willey et al. (2004) and Key et al. (2004) estimates do not include some adjacent seas and the Arctic Ocean, and their time axis are slightly shifted to prevent overlap. Note that IAF1 and IAF2 lines overlap.

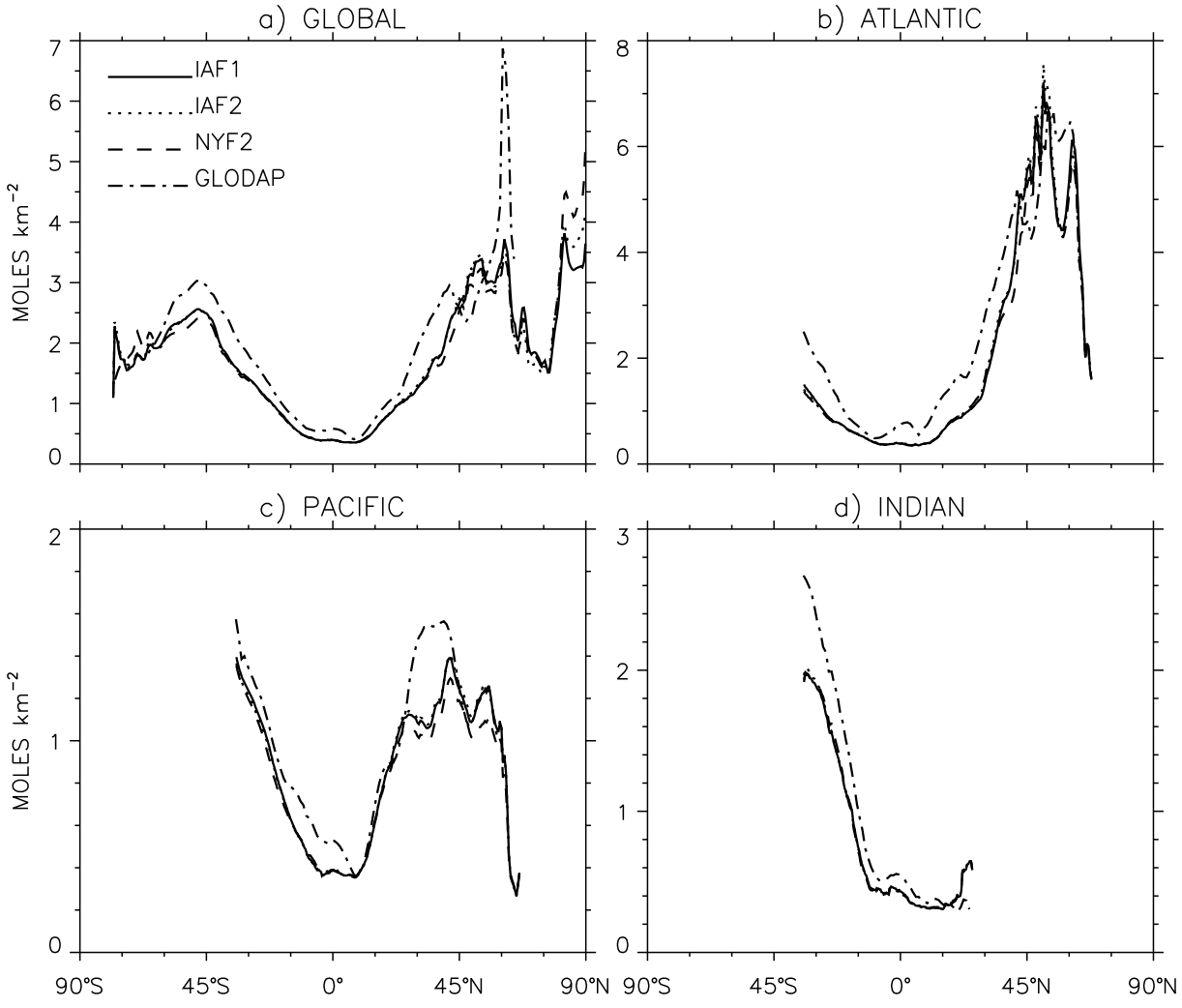

Figure 3. Zonal-mean CFC-11 column inventory for 1994 from model simulations and GLODAP data: a) Global, b) Atlantic, c) Pacific, and d) Indian Oceans.

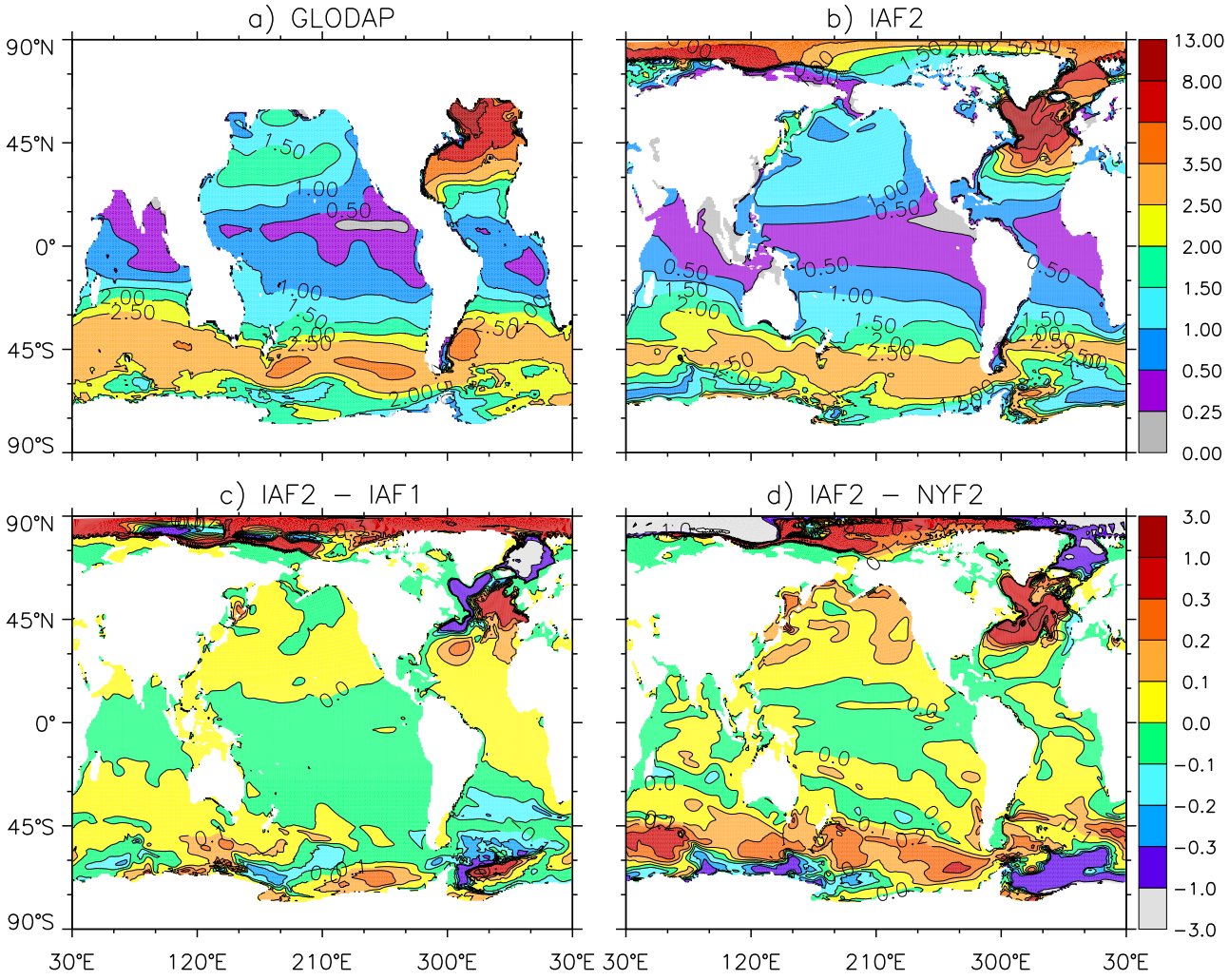

Figure 4. CFC-11 column inventory in moles km^{-2} for 1994 from a) GLODAP and b) IAF2; the model difference distributions for c) IAF2 − IAF1 and d) IAF2 − NYF2. Panels (a,b) and (c,d) share the same color bars, respectively.

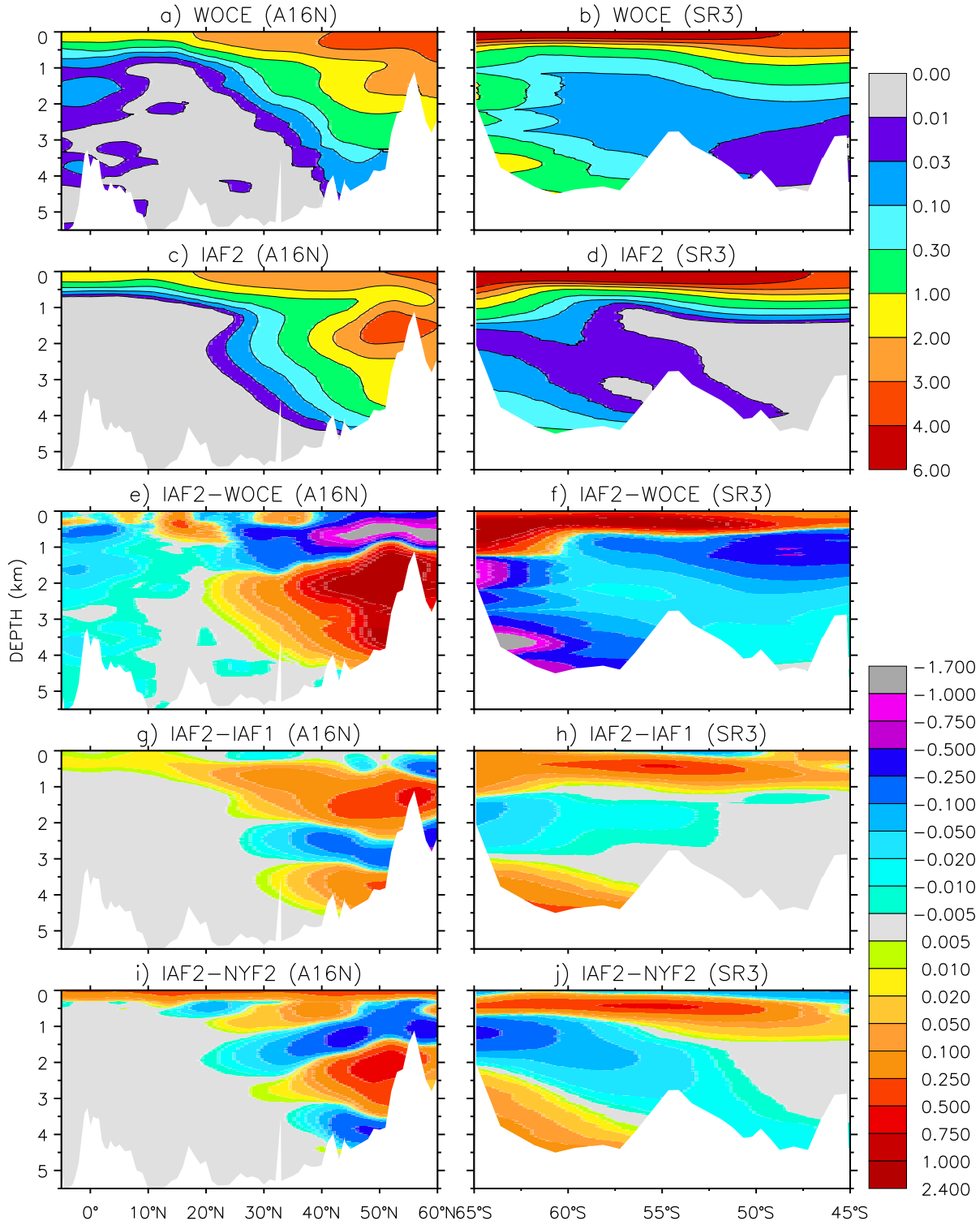

Figure 5. Observed and modeled CFC-11 distributions along WOCE sections A16N (20°W) for August 1993 (left panels) and SR3 (140°E) for October 1991 (right panels). For each section, IAF2 distribution along with IAF2 − WOCE, IAF2 − IAF1 and IAF2 − NYF2 difference distributions are shown. The unit is pmol kg^{-1}. Panels (a-d) and (e-j) share the same color bars, respectively. All panels use the same, observed topography.